Journal of Structural Geology, Vol. 14, No. 7, pp. 825 to 838, 1992
Printed in Great Britain

0191-8141/92 $05.00+0.00

Finite strain and deformation within the Briançonnais Castelvecchio–Cerisola nappe of the Ligurian Alps, Italy

SILVIO SENO

Dipartimento di Scienze della Terra dell' Università, Strada Nuova 65, 27100 Pavia, Italy

(*Received* 8 *May* 1991; *accepted in revised form* 27 *February* 1992)

Abstract—The structural history of the Castelvecchio–Cerisola Briançonnais nappe (Ligurian Alps, Italy) was dominated by a southwestward overthrust shear that resulted in isoclinal folding and schistosity-lineation fabric development within the nappe. This deformation was due to the intracontinental shortening related to the collision of the European and Adriatic plates during Late Cretaceous–Eocene times.

Finite strain, produced during the isoclinal folding and the schistosity-lineation fabric development, was determined from quartzites, conglomerates and tuffs using Fry's method. Strain type and intensities are strongly dependent on rock type: other factors, like the proximity to the major thrusts or the position in relation to the first phase recumbent folds, seem to be of secondary importance. The quartzites and conglomerates display a constrictional strain or else they approximate to plane strain, while the pyroclastic rocks fall into the field of apparent flattening and are characterized by a higher intensity of deformation.

During nappe emplacement the deformation was not accommodated by simple shear alone: the interpretation of strain patterns in the Castelvecchio–Cerisola has led to a model in which longitudinal strain was superposed on layer-parallel simple shear. Schistosity at a low angle to the major thrust faults, incremental extension directions deduced from pressure shadows, very frequent veins and stylolitic structures parallel to bedding support this hypothesis. The data presented here emphasize that subvertical thinning associated with thrust shear and a small extension perpendicular to the emplacement direction occurred in the Castelvecchio–Cerisola nappe.

INTRODUCTION

THE Ligurian Alps (Italy) represent the southernmost segment of the Western Alps (Fig. 1): eastward they are bounded by the Apenninic zone, while northwards they disappear under the Oligo-Miocene molassic cover. From Late Cretaceous to Upper Eocene, the subduction of the European palaeocontinent beneath the Adriatic plate, then the suture of the Piemont–Ligurian ocean, were accompanied by a considerable intracontinental crustal shortening. This was accomplished by means of a complex thrusting of both cover and basement nappes, which were displaced southwestwards (Vanossi 1980, Vanossi *et al.* 1986). Along an ideal section we find in ascending order: (1) Briançonnais units, derived from the European continent; (2) Piemont units, from its margin; and (3) ophiolitic units and Helminthoid Flysch nappes, from the Piemont–Ligurian oceanic domain. Westwards the nappe pile overlies outer, less deformed sequences (Dauphinois domain), representing the cover of the Argentera–Mercantour Massif.

This paper presents the results of a detailed analysis of one of the many nappes cropping out in the Ligurian Alps in order to investigate the strain mechanisms active during the nappe emplacement.

GEOLOGICAL SETTING

The Castelvecchio–Cerisola unit (CVC) is a Briançonnais nappe detached from its substratum at the Upper Permian level. Figure 2 schematically shows its stratigraphic sequence ranging up to Eocene. From a palaeogeographic point of view the Ligurian Briançonnais is traditionally divided into external, intermediate and internal domains from SW to NE, respectively. The

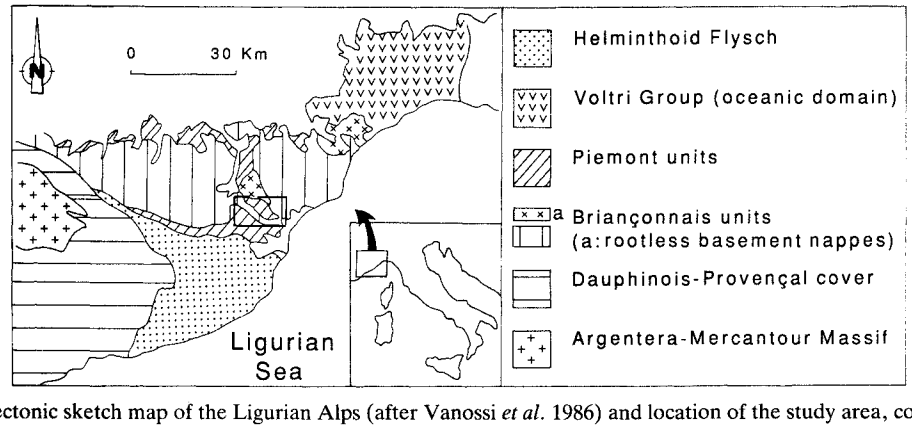

Fig. 1. Tectonic sketch map of the Ligurian Alps (after Vanossi *et al.* 1986) and location of the study area, corresponding to Fig. 6.

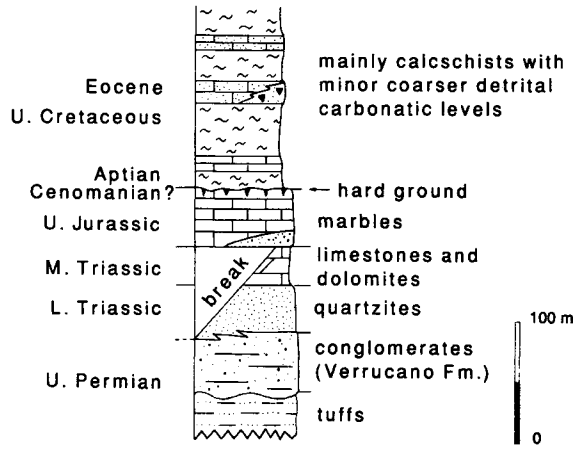

Fig. 2. Schematic stratigraphic section showing the position of quartzites, Verrucano conglomerates and tuffs.

position attributed to the CVC is intermediate–internal Briançonnais, that is near the European continental margin (Vanossi 1980).

The CVC overlies the lower Briançonnais units and is in turn overlain by the Piemont units (Fig. 3). Its thickness progressively decreases towards the east, where roof and basal thrust approach each other. Westwards it disappears under the Piemont units: where the lower Briançonnais units crop out again, they are not covered by the CVC, but directly by the Helminthoid Flysch nappe. The exposed part of the CVC is characterized by a general westward younging of the formations towards the nappe front. The CVC shows polyphase deformation under progressively decreasing metamorphic conditions: its top reached the Na-amphibole greenschist facies during the oldest deformation phase (Messiga *et al.* 1982).

DEFORMATION DURING NAPPE EMPLACEMENT

A pervasive S_1 foliation, developed parallel to bedding and to the nappe boundaries, is the dominant mesostructural element (Fig. 4): in the originally more pelitic rocks it is a slaty cleavage and in the Triassic or Jurassic calcareous layers it appears as a stylolitic cleavage. Jurassic marbles frequently show a stretching lineation (L_1) well documented by elongated diagenetic bands, intraclasts and minerals. The same lineation can be less frequently observed in the Verrucano.

The S_1 foliation runs parallel to the axial surfaces of tight folds (Fig. 4) that have transposed the lithological contacts and determined the tectonic setting of the whole nappe. These folds, sometimes cuspate, are common at the contact between Cretaceous–Eocene calcschists and Jurassic marbles where viscosity contrast is very high; they can have a wavelength of about 100 m with an amplitude of a few metres. F_1 mesoscopic folds usually fall into Ramsay's (1967) class 2 with a slight tendency towards class 3; the rounded hinge shown by lower amplitude folds suggest they started to develop by buckling processes. The interlimb angles vary between 0° and 90° with a mean of 30°. I have not been able to recognize sheath folds in the field, even when the F_1 folds are not cylindrical. Their axes are quite scattered, but in general have NW–SE orientations and are southwestward facing. The hinge regions of the largest recumbent structures are generally complicated and, in these localities, the stratigraphic sequence is repeated many times.

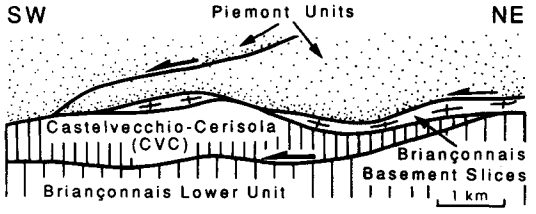

Fig. 3. Sketch section showing the tectonic position of the CVC below the Piemont units and above a lower, more external, Briançonnais unit.

The observation of asymmetric structures, such as pressure shadows around clasts, *S–C* fabrics and shear bands at a high angle to foliation (Berthé *et al.* 1979, Simpson & Schmid 1983, Lister & Snoke 1984, Passchier & Simpson 1986), indicates that the deformation was rotational and that the displacement was top-to-the-SW.

POST-NAPPE DEFORMATIONS

The thrust contacts between the CVC and the other units, as well as the structures described above, are affected by later folding. F_2 folds are present from microscopic to regional scale, they are asymmetric, overturned to the north or northeast and have axes trending SE–NW. The interlimb angles vary from 20° up to 120° in the more competent layers, with a mean of about 60°.

Flattened parallel folds (Ramsay's 1C class) are dominant in dolomites, marbles and quartzites. In the Cretaceous–Eocene calc-schists class 1C folds alternate along the same axial plane with class 3. These fold sets are characteristically polyharmonic or disharmonic. F_2 folds were formed by a combination of flexural-slip and layer-parallel shortening (Seno 1988). The interference with the first-phase structures gives rise to class 3 interference pattern (Ramsay 1967), corresponding to the G case of Thiessen & Means (1980). The axial plane foliation of F_2 folds is a well-developed crenulation cleavage in rocks showing strong S_1 foliation, it dips constantly to the south or southwest and produces asymmetric microlithons (Fig. 4). These structures, affecting all tectonic units from the deepest to the highest, represent a distinct deformational event resulting in a general reversal of the shear direction.

The last stage of ductile deformation is represented by gentle folding characterized by steep axial planes, trending N–S, normal to the chain. The interference of F_3 and F_2 folds produces large-scale asymmetrical domes and basins. This kind of interference gave rise to the outcrop pattern of pre-Cretaceous terrains below the calc-schists

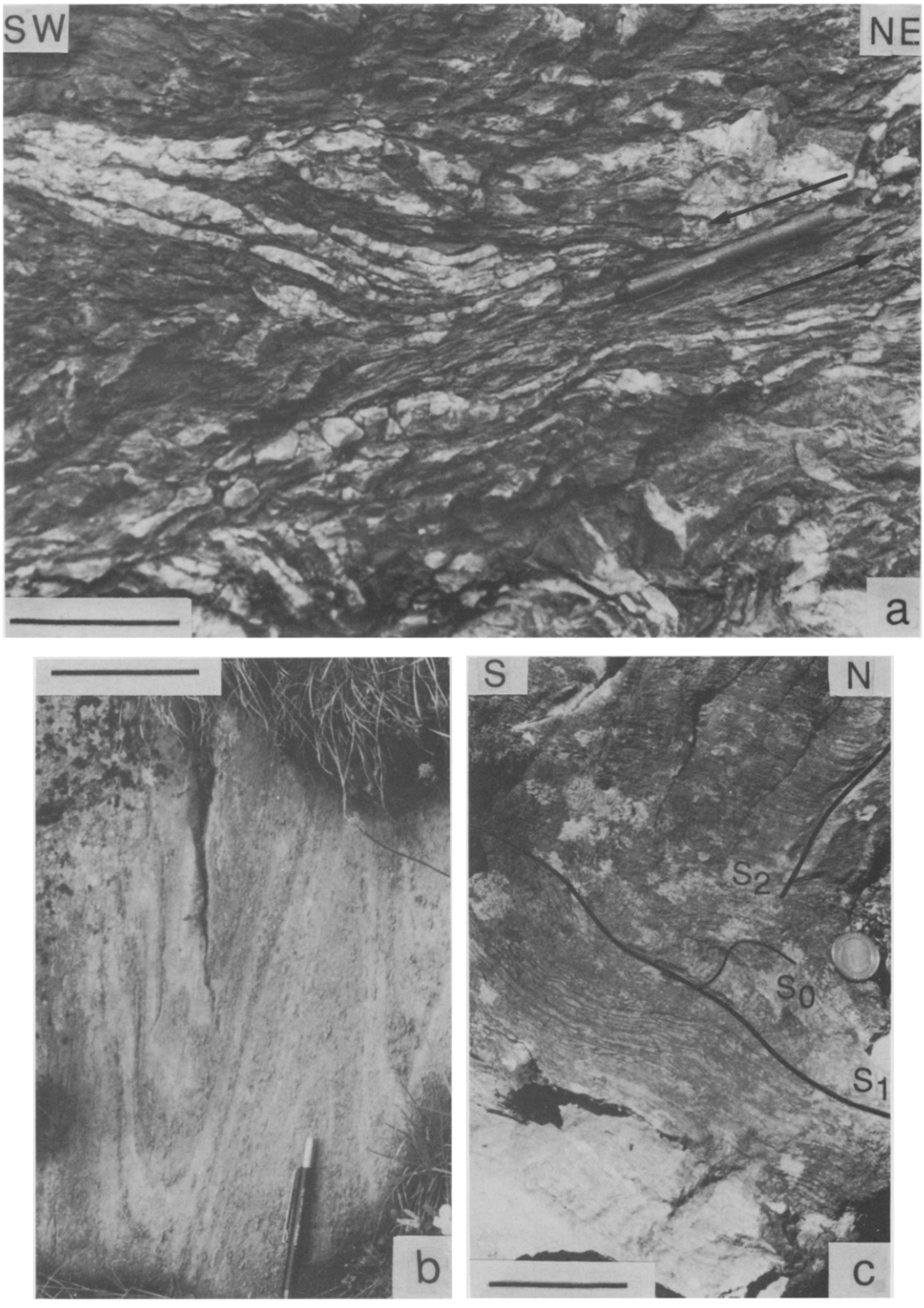

Fig. 4. (a) Sinistral shear zone in the Upper Cretaceous–Eocene calc-schists. (b) F_1 fold in Jurassic marbles. (c) Superposed foliations in the Upper Cretaceous–Eocene arenaceous layers. Scale bar equals 10 cm in all photographs.

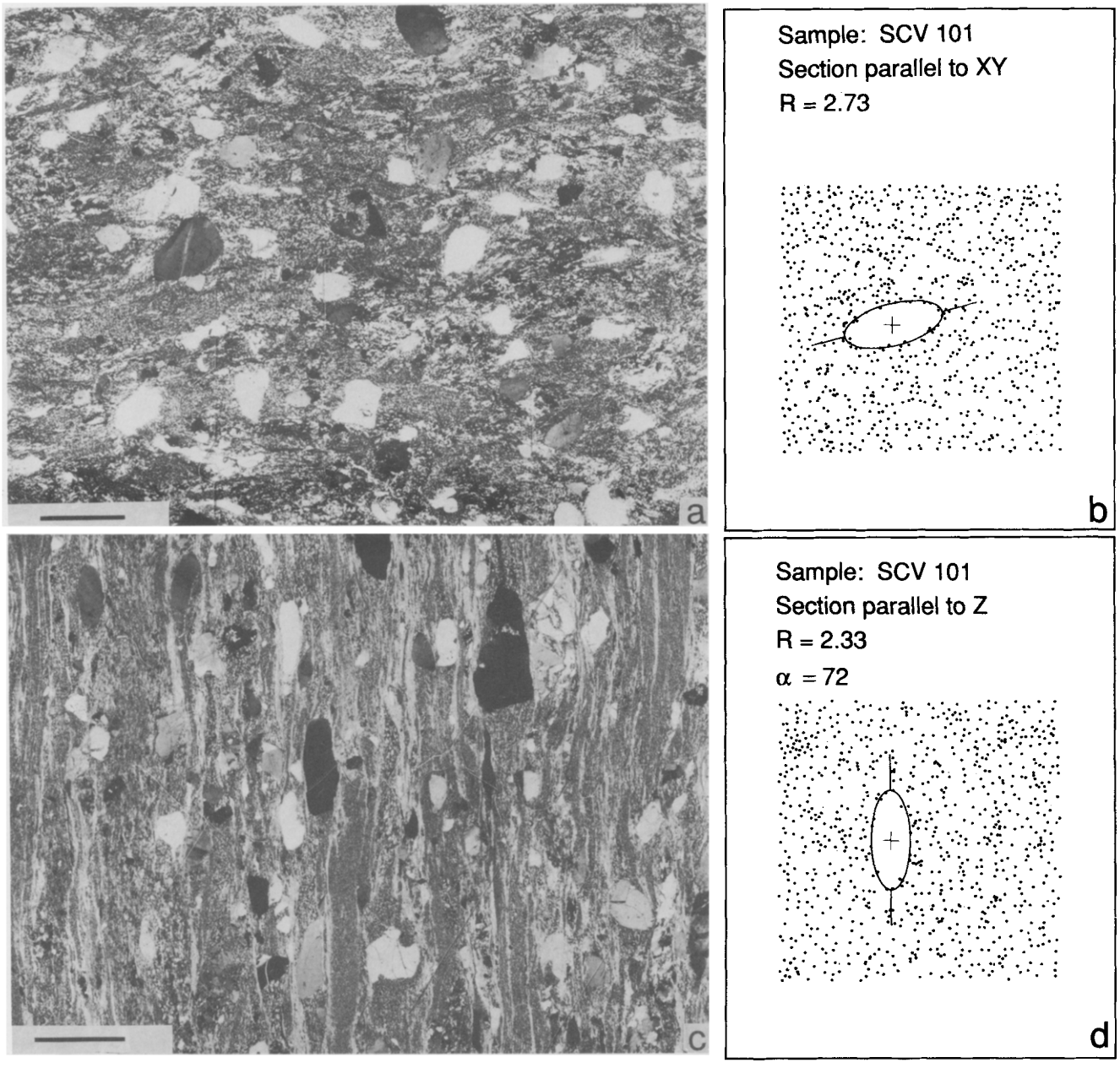

Fig. 5. Example of two-dimensional strain data obtained from the Fry method: Permian tuffs. R is the strain ratio and α is the angle between the X direction and the intersection of the section parallel to Z with the XY principal plane (see text). In (a) and (c) quartz grains display a low degree of intracrystal plasticity and the absence of subgrains at boundaries. Scale bar equals 1 mm; crossed nicols.

and of the CVC itself. Mesoscopic F_3 folds are rare and they usually lack a good axial plane foliation.

Brittle deformations are mostly represented by E–W-trending normal faults clearly intersecting F_3 folds. Although these faults cannot be directly dated, they are probably related to the well known Pliocene–Quaternary extensional system (Consiglio Nazionale delle Ricerche 1983) responsible for the structure of the Ligurian coast.

SAMPLE DESCRIPTION

Finite strain has been determined from different rock types within the Permo-Triassic portion of the CVC succession. Rhyodacitic tuffs, with phenoclasts of quartz, minor K-feldspar and plagioclase, are located in the lower part of the CVC succession. They are overlain by conglomerates with pebbles of mainly quartzite and red rhyolite (Verrucano Formation). They are continental deposits characterized by clasts which size ranges from few millimetres to 10 cm, and their matrix, which is sometimes very abundant, consists largely of quartz. Most of the samples which belong to the Verrucano were taken from micro-conglomeratic facies. The Verrucano, in turn, is covered by a layer of well-sorted Lower Triassic quartzites without matrix, which represent beach deposits. Both the pyroclastic rocks and the Verrucano are well foliated and the dominant foliation at all localities is S_1.

Microstructures and deformation mechanisms

Pyroclastic deposits, continental conglomerates and quartzites display different microstructures developed during the emplacement of CVC. Quartz grains of quartzites, characterized by a low percentage of matrix, show a variable degree of crystal plasticity; strong undulatory extinction, deformation bands, deformation lamellae and core-and-mantle structures are common features. Deformation is reached, at least partially, by means of grain-size reduction and grain-boundary sliding. Grain-size reduction may be substantial, but the rocks do not reach a high degree of mylonitization: crystals have a low length–width ratio, often less than 2:1, globular individuals are frequent and few grains are completely replaced by subgrains. The above structures in general correspond with low finite strain values.

In pyroclastic rocks and Verrucano conglomerates the matrix is abundant. S_1 foliation is well marked by clastic micas and recrystallized phyllosilicates aligned parallel to it. Quartz–feldspar clasts show a well-defined preferred orientation of their long axes, but the degree of crystal plasticity is very low (Fig. 5). Quartz grains are characterized by weak undulatory extinction and are, at most, affected by deformation bands and lamellae; the grain boundaries are mostly free of subgrains. Feldspar clasts are subordinate and usually fractured. As in the Lower Triassic quartzites, deformation has been partially accommodated by means of intragranular slip, both between clast fragments and in the matrix along mica enriched shear bands.

All of the rock types show evidence suggesting pressure solution as an important deformation mechanism: some quartz grain contacts are stylolitic; many clasts are truncated by mica layers; pressure shadows around clasts or between clast fragments are commonly observed and represent the most prominent microscopical feature of tuffs and Verrucano (Fig. 5). Pressure shadows help define the main foliation in thin sections, where they are most common and suggest continuous mass transfer of silica from the matrix. The above-mentioned microstructural association, typical of deformation at low temperature (Tullis *et al.* 1973), is in agreement with the low-grade regional metamorphism (Messiga *et al.* 1982).

FINITE STRAIN ANALYSIS

Two-dimensional analysis

All two-dimensional strain analyses (Table 1) were made in the laboratory on thin sections or polished surfaces. Only samples showing no cleavages due to deformations post-dating the main foliation event were used, thus the computed finite strains should largely reflect the oldest deformation (D_1) of nappe emplacement.

Before undertaking regional work, comparative strain estimates were made from seven samples (14 sections) of tuffs, conglomerates and quartzites in order to determine the most suitable and reproducible method. Between 100 and 200 grains were used for the measurements of axial ratios (R_f) and long-axis orientations (ϕ) by the method of θ-curves (Lisle 1977, Peach & Lisle 1979), tensor averaging (Shimamoto & Ikeda 1976) and of Fry centre-to-centre method (Fry 1979, Hanna & Fry 1979). On the sections perpendicular to the schistosity, where the strain ratios were higher and the variation in long axis orientation very low, the Shimamoto & Ikeda estimates were slightly higher than the other two. On the XY sections, the results obtained with the R_f/ϕ techniques were in reasonable agreement with each other and they were lower than those which Fry's method provided.

For subsequent measurements, the Fry's method was used for the following reasons.

(1) Chi-square tests applied to some pyroclastic rocks gave values above the critical level, which suggests the presence of either a competence contrast between clasts and matrix or a pretectonic fabric.

(2) In most of the samples collected, there is evidence of a viscosity contrast between clasts and matrix: the foliation is deflected around clasts or phenoclasts and the presence of pressure shadows is very common (Fig. 5).

To have enough grain centres it was usually necessary

Table 1. Two-dimensional strain data. *IZ* are sections parallel to *Z*. F, Fry method; S & I, Shimamoto and Ikeda method; Th, θ-curves method. Pitch of *X* axis is taken clockwise from strike; α is the angle between the *X* direction and the intersection of the section parallel to *Z* (*IZ*) with the *XY* principal plane

Sample	Rock type	Section	Method	R	Orientation (az/pl)	Pitch of *X*	α
SCV 67	Tuff	XY	F	2.10	286/28	16	—
		IZ	F	2.75	—	—	37
SCV 70	Tuff	XY	F	1.52	340/27	102	—
		IZ	F	2.40	—	—	75
SCV 71	Conglomerate	XY	F	2.00	007/23	99	—
		IZ	F	2.40	—	—	38
SCV 72	Conglomerate	XY	F	2.33	002/38	90	—
		IZ	F	2.35	—	—	62
SCV 73	Tuff	XY	F	2.11	002/22	82	—
		IZ	F	2.00	—	—	75
SCV 74	Quartzite	XY	F	3.20	107/13	24	—
		IZ	F	4.64	—	—	0
SCV 76	Conglomerate	XY	F	2.33	160/30	127	—
		IZ	F	2.47	—	—	75
SCV 77	Conglomerate	XY	F	4.59	204/55	73	—
		IZ	F	2.29	—	—	73
SCV 78	Conglomerate	XY	F	3.18	322/48	14	—
		IZ	F	2.17	—	—	35
SCV 79	Tuff	XY	F, S & I, Th	1.87	204/78	160	—
		IZ	F, S & I, Th	3.30	—	—	40
SCV 80	Conglomerate	XY	F	1.86	339/60	74	—
		IZ	F	2.50	—	—	43
SCV 81	Conglomerate	XY	F, S & I, Th	1.26	160/10	120	—
		IZ	F, S & I, Th	2.38	—	—	66
SCV 83	Conglomerate	XY	F	2.20	244/44	90	—
		IZ	F	1.27	—	—	83
SCV 84	Tuff	XY	F	1.73	325/27	178	—
		IZ	F	2.42	—	—	75
SCV 85	Tuff	XY	F	1.70	010/50	176	—
		IZ	F	2.53	—	—	90
SCV 86	Quartzite	XY	F	1.56	230/40	18	—
		IZ	F	1.33	—	—	78
SCV 87	Conglomerate	XY	F	1.68	280/49	11	—
		IZ	F	1.67	—	—	5
SCV 88	Conglomerate	XY	F	2.31	303/60	166	—
		IZ	F	2.33	—	—	20
SCV 89	Quartzite	XY	F	1.71	050/31	63	—
		IZ	F	2.00	—	—	90
SCV 90	Conglomerate	XY	F	1.78	165/13	129	—
		IZ	F	2.75	—	—	75
SCV 91	Tuff	XY	F	2.00	019/68	92	—
		IZ	F	2.10	—	—	75
SCV 92	Conglomerate	XY	F	2.35	220/50	78	—
		IZ	F	2.33	—	—	64
SCV 93	Conglomerate	XY	F	2.00	218/60	94	—
		IZ	F	1.59	—	—	56
SCV 94	Tuff	XY	F	1.55	189/64	141	—
		IZ	F	4.10	—	—	90
SCV 96	Tuff	XY	F	3.37	016/14	110	—
		IZ	F	4.67	—	—	65
SCV 97	Conglomerate	XY	F	2.00	075/10	17	—
		IZ	F	2.92	—	—	21
SCV 98	Tuff	XY	F	1.58	170/4	28	—
		IZ	F	2.48	—	—	70
SCV 99	Conglomerate	XY	F	2.00	156/20	112	—
		IZ	F	3.14	—	—	22
SCV 100	Tuff	XY	F	1.50	225/30	90	—
		IZ	F	2.38	—	—	80
SCV 101	Tuff	XY	F, S & I, Th	2.73	286/20	5	—
		IZ	F, S & I, Th	2.33	—	—	72
SCV 102	Tuff	XY	F	1.41	346/10	130	—
		IZ	F	3.68	—	—	25
SCV 104	Conglomerate	XY	F	1.91	112/28	53	—
		IZ	F	2.07	—	—	10
SCV 105	Tuff	XY	F	2.00	235/39	36	—
		IZ	F	4.71	—	—	85
SCV 106	Conglomerate	XY	F, S & I, Th	2.50	233/35	80	—
		IZ	F, S & I, Th	2.43	—	—	64
SCV 109	Conglomerate	XY	F	2.50	359/46	165	—
		IZ	F	2.00	—	—	10
SCV 110	Conglomerate	XY	F	2.00	330/72	16	—
		IZ	F	2.94	—	—	0
SCV 111	Conglomerate	XY	F, S & I, Th	1.63	286/20	178	—
		IZ	F, S & I, Th	1.65	—	—	82
SCV 112	Conglomerate	XY	F, S & I, Th	1.50	329/44	160	—
		IZ	F, S & I, Th	3.43	—	—	30
SCV 113	Tuff	XY	F, S & I, Th	1.53	065/55	103	—
		IZ	F, S & I, Th	5.43	—	—	11

to use all of the surface of a standard thin section and the best-fitting cut-off ellipses were established visually, directly on the Fry plot. Almost all of the diagrams were of good quality after having plotted 80–100 centres. Using a greater number of objects, the central vacancy was better defined, without undergoing notable variation. The measured ellipse axes are always parallel to the macro or microscopic fabric axes (extension lineation, trace of schistosity). This supports an initial random uniform centres distribution and homogeneous deformation on the scale of thin section.

The simplicity and elegance of Fry's method has encouraged its use with a wide range of rocks (Stone & Schwerdtner 1981, Lacassin & van den Driessche 1983, Schwerdtner *et al.* 1983, Siddans *et al.* 1984) even if it has some limitations. Since the original object distribution must be two-dimensionally anticlustered (Ramsay & Huber 1983), the more it departs from this distribution and tends to be random, the more the resulting strain ellipse becomes ambiguous; the strain ellipse becomes impossible to define in the case of a random (Poisson) distribution (Fry 1979). Crespi (1986) estimated that the number of points required by poorly anticlustered distributions should range from 200 to 800. The normalized analysis of packed aggregates proposed by Erslev (1988), which eliminates this disadvantage and produces a better defined strain ellipse, cannot be applied to unpacked aggregates like the quartz–feldspar grains considered in the present strain determination.

Three-dimensional analysis

To obtain the constant volume strain ellipsoid, the strain ratios and orientations were determined, for each oriented sample, on two mutually perpendicular sections. The first section was cut parallel to the XY plane ($X \geq Y \geq Z$), assuming the main foliation to be coincident to it; the second (IZ section) was cut perpendicular to the XY plane and was not coincident with a principal plane of the strain ellipsoid, but contained the Z axis: the major ellipse axis (I) on this second section is intermediate between X and Y.

The Fry method yields axial ratios, nevertheless the relative stretches on different sections can be standardized with respect to one of the principal strains (namely X) assigning an arbitrary value to it. The length of the major axis of the ellipse in the IZ section is related to the strains on the XY plane in the following fashion (Ramsay & Huber 1983, equation 6.4):

$$1/I^2 = \cos^2 \alpha/X^2 + \sin^2 \alpha/Y^2$$

then

$$Z^2 = I^2/R_{IZ}^2,$$

where α is the angle that the X direction makes with the intersection of the IZ section with the XY principal plane; X, Y, Z are relative stretches; R_{IZ} and I are, respectively, the strain ratio and the maximum relative stretch on the IZ section.

FINITE STRAIN RESULTS

Finite strain measurements within the CVC were made at 39 localities (Fig. 6). The principal strains X, Y, and Z, normalized to the constant volume ellipsoid, are listed in Table 2 together with X and Z orientations and $K = \ln(X/Y)/\ln(Y/Z)$. All the calculated ellipsoids have been plotted on a logarithmic deformation diagram (Fig. 7a). The straight line of unit slope $\Delta = 0\%$ (no volume change) divides the apparent constriction field from that of apparent flattening. The samples were separated according to their lithology and their structural position with respect to the large recumbent folds. Although they are not uniformly distributed (only nine belong to inverted limbs) it is immediately possible to see that the type of strain is not directly related to the structural position, since the constrictional ellipsoids appear on both normal and on inverted limbs.

The distribution on the Flinn plot seems to be controlled by lithology. The tuffs and strongly matrix-supported conglomerates tend to give flattened ellipsoids, while the quartzites and conglomerates without phyllosilicates in the matrix approximate to plane strain or fall in the field of constriction. As a centre-to-centre method has been used, the preceding results reflect the 'whole-rock' strain: the final ellipsoid shapes are not influenced by the different behaviour of the objects, e.g. viscosity contrast between object and matrix.

The intensity of the strain was defined using the parameter $\bar{\varepsilon}_s$ (Ramsay & Huber 1983) (Table 2), then plotted in Fig. 7(b) against Lode's parameter (Hossack 1968). Two things stand out: (a) the $\bar{\varepsilon}_s$ values normally remain quite low throughout the nappe and (b) the intensity of the strain increases with increasing Lode's parameter.

The finite strain results resemble those carried out in the Jurassic marbles of the Caprauna–Armetta Briançonnais nappe (Menardi Noguera 1988), whose tectonic position is comparable with that of the CVC and which represent the only other strain data available for the Ligurian Alps. The higher strain intensity characterizing the Caprauna–Armetta, which was deformed under lower metamorphic conditions, is related to: (1) the higher viscosity of Jurassic marble in comparison with Permotriassic rocks of the CVC; and (2) the geometry of the Caprauna–Armetta, which is a fold nappe characterized by very high X/Z ratio on its well-developed inverted limb.

Strain orientations

Figures 8–10 show aspects of the orientation of the principal strains. The X axes trend from NE to SW, more or less parallel to the stretching lineation (L_1); the calculated best-fit directional vectors of X axes and L_1 lineations almost have the same orientations (Fig. 10). The second-phase folds rotate X and L_1 leading to plunge variations because F_2 axes and L_1 lineations are approximately orthogonal. The largest deviations of the extension directions from NE to SW are ascribed to the

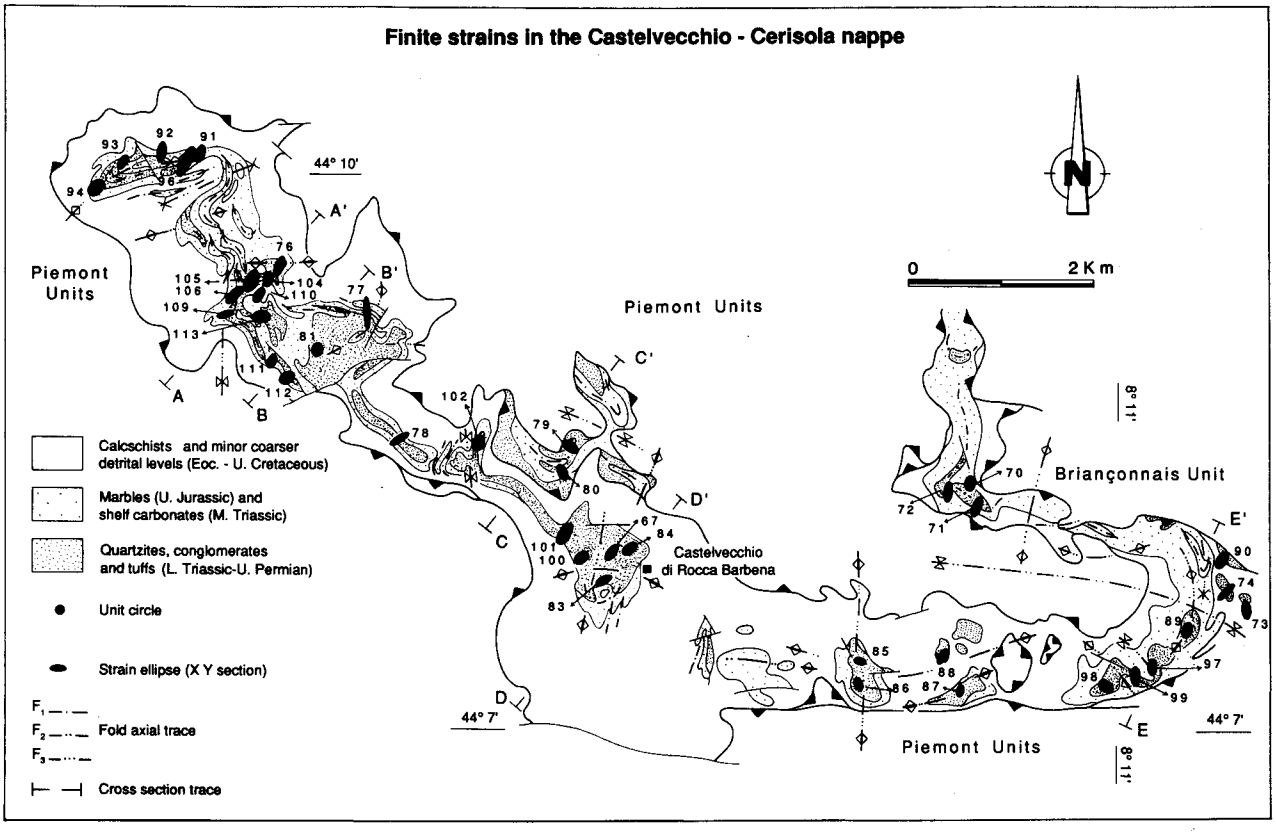

Fig. 6. Simplified geological map of the CVC unit showing orientation of strain ellipsoid XY sections. Numbers refer to the sampling sites.

interference with N–S-trending F_3 folds and are mostly localized in the eastern sector, where interference is well documented at the map scale (Seno 1988).

It is, however, possible to note that the X axes are more scattered with respect to the extension lineation poles: this could depend on small errors in the strain analysis which, in samples of low deformation, can cause very notable variations in orientation. Secondly, it is important to underline the fact that almost all the extension lineation attitudes, shown in Fig. 10, were measured in the Jurassic marbles and not in the same rocks and sites of the strain analysis. In Fig. 10 it is also possible to note that the dispersion of Z axes is comparable to that of poles to the main foliation: both have a girdle distribution due to the second-phase post-nappe folds whose axes are oriented NW–SE. The agreement between the axes derived from strain analysis and the ones of the mesoscopic fabric represents a good check for strain analysis itself.

Pressure shadows

Pressure shadows around quartz–feldspar clasts are common: they are sealed by quartz and white mica fibres disposed parallel to the incremental extension orientation. Sometimes both quartz and feldspar clasts are fractured and these fractures are sealed by quartz. Fibres are always deformed and dynamically recrystallized, therefore they provide only qualitative observations.

In sections parallel to schistosity (XY) the extension directions are largely straight and are consistent with the X directions calculated using Fry's method. Only some samples, lying in the flattening field, are weakly extended along Y and in this case some clasts underwent 'chocolate tablet' boudinage (the estimated extension in Y can reach 20%); this observation is confirmed by vein systems showing extension parallel to X but not appreciably to Y (Seno & Turrini 1989). Pressure shadows are very well developed and often asymmetric on sections more or less parallel to XZ: however, they are nearly absent from sections more or less parallel to YZ.

Strain components

The CVC makes up part of a pile of nappes which are separated by overthrust surfaces (Vanossi *et al.* 1986), and so its internal deformation should be of plane strain. The presence of oblate and prolate ellipsoids leads to the discussion of the problem of strain factorization.

The presence of a large number of flattened ellipsoids and the fact that they specially occur in tuffs, raises the question of how much the final ellipsoid shapes can be due to volume loss. To calculate the maximum possible volume loss the oblate ellipsoids have been algebraically decomposed into compaction (no extension along X and Y) and plane strain components (Sanderson 1976): the latter is considered to be due to layer-parallel simple shear, as suggested by the low angle between bedding and schistosity.

On the basis of this assumption, estimated volume losses (Table 3), expressed in terms of shortening along

Table 2. Finite strain results: X, Y and Z are normalized to constant volume ellipsoid equal to $4\pi/3$. $K = \ln(X/Y)/\ln(Y/Z)$. ν and $\bar{\varepsilon}_s$ defined in Fig. 7(b)

	Normalized finite strain ellipsoids							
Sample	X	Y	Z	X (az/pl)	Z (az/pl)	K	ν	$\bar{\varepsilon}_s$
SCV 67	2.05	0.98	0.50	210/07	106/62	1.10	−0.09	1.00
SCV 70	1.75	1.15	0.49	353/26	160/63	0.49	0.61	0.92
SCV 71	1.92	0.96	0.55	017/26	187/67	1.23	−0.21	0.89
SCV 72	2.27	0.97	0.45	002/38	182/52	1.10	−0.10	1.14
SCV 73	2.05	0.97	0.50	354/22	182/68	1.14	−0.12	1.00
SCV 74	2.46	0.77	0.53	040/05	287/77	3.14	−0.81	1.13
SCV 76	2.35	1.01	0.42	198/16	340/70	0.95	0.04	1.22
SCV 77	3.63	0.79	0.35	176/52	024/35	1.88	−0.56	1.68
SCV 78	2.39	0.75	0.55	241/10	142/42	3.74	−0.87	1.10
SCV 79	2.06	1.10	0.44	290/20	024/12	0.68	0.36	1.11
SCV 80	1.89	1.02	0.52	309/56	159/30	0.93	0.09	0.91
SCV 81	1.54	1.22	0.53	190/09	340/80	0.28	0.85	0.79
SCV 83	1.82	0.83	0.66	244/44	064/46	3.43	−0.84	0.75
SCV 84	1.92	1.11	0.47	051/02	145/63	0.64	0.42	1.00
SCV 85	1.94	1.14	0.45	096/02	190/40	0.57	0.51	1.05
SCV 86	1.47	0.94	0.72	154/12	050/50	1.67	−0.47	0.51
SCV 87	1.41	0.84	0.84	197/08	100/41	∞	−1.00	0.42
SCV 88	1.88	0.81	0.66	020/05	123/30	4.20	−0.89	0.78
SCV 89	1.80	1.05	0.53	020/07	230/59	0.79	0.23	0.87
SCV 90	2.04	1.15	0.43	205/10	345/77	0.58	0.49	1.11
SCV 91	2.02	1.01	0.49	024/68	199/22	0.96	0.04	1.00
SCV 92	2.29	0.97	0.45	202/49	040/40	1.12	−0.01	1.15
SCV 93	1.77	0.89	0.64	226/60	038/30	2.09	0.63	0.73
SCV 94	2.15	1.39	0.34	260/34	009/26	0.31	0.83	1.36
SCV 96	3.67	1.09	0.25	036/13	196/76	0.82	0.19	1.90
SCV 97	1.80	0.90	0.61	002/03	255/80	1.77	−0.52	0.78
SCV 98	1.81	1.15	0.48	108/02	350/86	0.52	0.57	0.95
SCV 99	1.96	0.98	0.52	180/20	336/70	1.10	−0.09	0.94
SCV 100	1.74	1.16	0.49	225/30	045/60	0.48	0.64	0.92
SCV 101	2.41	1.05	0.39	197/05	106/70	0.84	0.17	1.29
SCV 102	1.77	1.26	0.45	026/08	166/80	0.33	0.80	1.01
SCV 104	1.60	0.84	0.74	071/22	292/62	4.92	−0.92	0.58
SCV 105	2.64	1.32	0.29	208/36	055/51	0.45	0.65	1.60
SCV 106	2.40	0.96	0.43	220/36	053/55	1.15	−0.13	1.22
SCV 109	1.86	0.74	0.72	074/15	179/44	30.64	−0.10	0.76
SCV 110	1.80	0.90	0.61	245/15	150/18	1.78	−0.52	0.78
SCV 111	1.64	1.01	0.61	013/02	106/70	0.96	0.04	0.70
SCV 112	1.80	1.20	0.46	044/14	149/46	0.43	0.70	0.99
SCV 113	2.04	1.33	0.37	087/53	245/35	0.34	0.80	1.26

Z, range from −0.02 to −57%, with a mean value of −30%. As far as the tuffs are concerned, volume losses even higher than 50% are possible, but, on average, they are around 40% (Roberts & Siddans 1971): the values obtained could therefore be theoretically possible. Examination of the data from individual samples shows that some conglomerates also fall decidedly in the flattening field: for example, the SCV 81 and 112 samples (Verrucano) should have undergone a volume reduction of 45 and 43%, respectively. Such volume loss due to compaction is quite difficult to envisage in quartzite and Verrucano because the original lithology was heterogeneous, ranging from well sorted beach sands to fluvial conglomerates and poorly sorted sands with a high percentage of matrix. Nevertheless it is likely that the pre-tectonic compaction varies from very little in quartzites up to 20% in conglomerates (Athy 1930, Perrier & Quiblier 1974, Baldwin & Butler 1985). On Fig. 7(a) the straight lines labelled $\Delta = 20\%$ and $\Delta = 40\%$ separate the true flattening from the true constriction field for deformation preceded by such volume losses.

If the calculated volume reductions represent the maximum values it follows that the tectonic strain values listed in Table 3 represent minimum estimates. The factorization into pre-tectonic compaction and simple shear, however, is clearly not enough to be able to explain the existence, in some samples, of a real extension in the Y direction and, since the schistosity is always at a low angle with the bedding, the presence of a prolate ellipsoid. In order to discuss a more realistic model the possibility of a combination of simple and pure shear was checked with the technique described by Coward & Kim (1981), Kligfield *et al.* (1981) and Sanderson (1982). For 11 samples of the CVC, the XZ axial ratios and the angles between the X axes and the nappe boundaries, were plotted on the strain chart in Fig. 11: all the other samples were discarded because the excessive distance from the shear-zone boundaries and the presence of small-scale post-nappe fold made the angular measurements unreliable.

The pressure shadows indicate that the last strain increments correspond to an extension in the Y direction. As there is no geological evidence to attribute this extension to a progressive rotation of the displacement direction or to the presence of an important wrench shear component, the deformation associated with the emplacement of the CVC was considered a combination of layer-parallel simple shear followed by pure shear. In

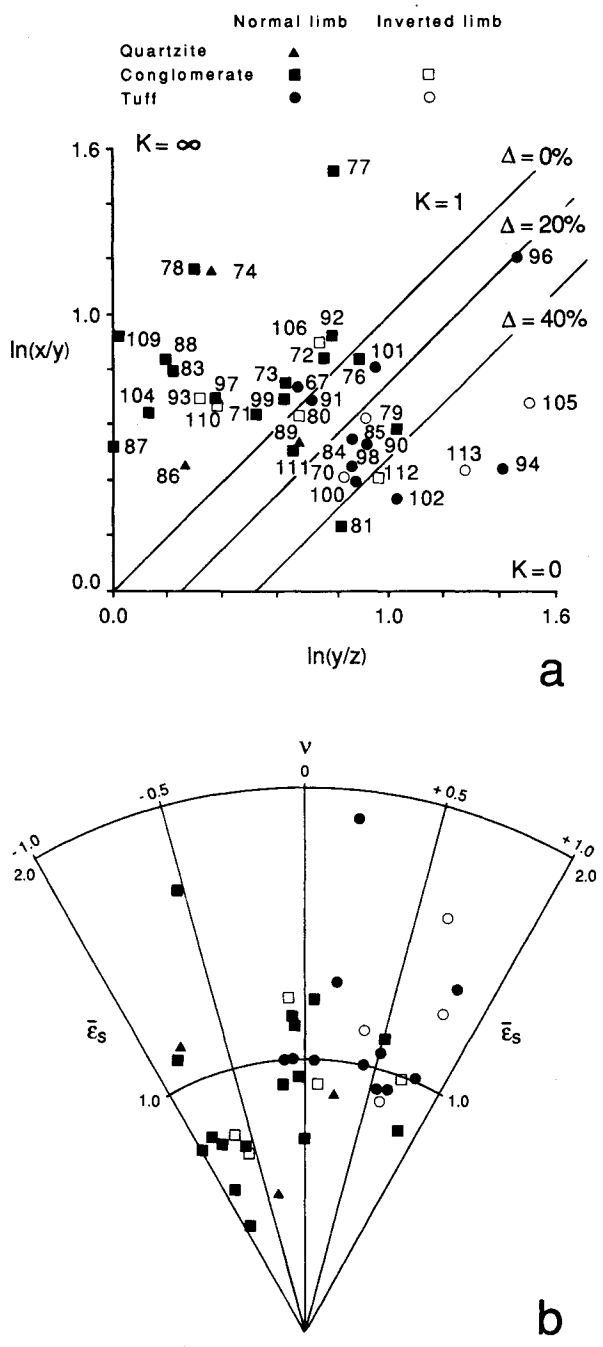

Fig. 7. (a) Logarithmic deformation plot of CVC finite strain data; straight lines corresponding to plane strain for 0, 20 and 40% volume loss are showed. $K = \ln(X/Y)/\ln(Y/Z)$. Sample numbers as in Table 1. (b) Polar graph of the strain parameter $\bar{\varepsilon}_s$ vs Lode's parameter ν.

$$\nu = \frac{2\varepsilon_2 - \varepsilon_1 - \varepsilon_3}{\varepsilon_1 - \varepsilon_3} \quad \text{(Hossack 1968);}$$

$$\bar{\varepsilon}_s = \frac{1}{\sqrt{3}}[(\varepsilon_1 - \varepsilon_2)^2 + (\varepsilon_2 - \varepsilon_3)^2 + (\varepsilon_3 - \varepsilon_1)^2]^{1/2}$$

(Ramsay & Huber 1983).

this model, on a plane which is perpendicular to the layers and parallel to the shear direction, the deformation is expressed by:

$$\begin{vmatrix} \sqrt{\lambda} & \sqrt{\lambda}\gamma \\ 0 & 1/\sqrt{\lambda} \end{vmatrix},$$

where γ is the shear strain, $\sqrt{\lambda}$ and $1/\sqrt{\lambda}$ are the stretches, respectively, parallel and perpendicular to the shear direction.

Plotting the curves for different values of γ and λ together with the CVC data, we can observe in Fig. 11 that the amounts of shear strain are low and quite homogeneous ($0.25 \leq \gamma \leq 1.5$): what is more, all of the samples lie below the curve $\lambda = 1$ and so show an extra extension parallel to X varying from $\lambda = 1.2$ to $\lambda = 3$. This type of factorization does not take the pre-tectonic compaction into account: in any case, almost all of the samples plotted are either conglomerates or quartzites and, so, they should be characterized by little pre-tectonic volume reduction.

DISCUSSION

The deformation of the CVC can be interpreted as a simple-shear regime on the base of the following evidence: (1) the unit is detached from its pre-Permian substratum, inserted in a pile of nappes stratigraphically differentiated with respect to it and bounded by two thrust surfaces; (2) the schistosity inside the CVC makes a low angle with major thrust faults and is subparallel to the layers; (3) first-phase folds are tight to isoclinal and their uniform asymmetry is consistent with 'top-to-the-SW' sense of shear; and (4) rotated clasts and shear-sense indicators are commonly present. In spite of observations that indicate simple-shear deformation, most of the studied samples show even greater deviation from plane strain, excluding the possibility of deformation by simple shear alone.

Interpretation of the results

A large portion of the observable strain in the quartzites, conglomerates and tuffs of the CVC was produced during isoclinal folding and schistosity-lineation fabric development. The Fry method shows that the strain is heterogeneous and displays a strong dependence on rock type: other factors like the proximity to the major thrusts or the position relative to the first phase folds, seem to be of secondary importance. The quartzites and conglomerates show a constrictional strain or else they approximate to the plane strain, while the tuffs fall decidedly into the field of apparent flattening and are characterised by a higher intensity of the deformation. In the latter, a reasonable volume reduction would be between 30 and 40%.

The final ellipsoids have been considered in terms of a combination of volume loss, simple shear and longitudinal strain: not enough data are available to consider all three factors together. The results point to the presence of a variable amount of extra extension in the X direction probably due to pure shear perpendicular to the layering, as indicated by foliation subparallel to the layering and by pressure shadows which underline a weak extension in the Y direction. Moreover the presence of extensive pressure solution in the whole nappe

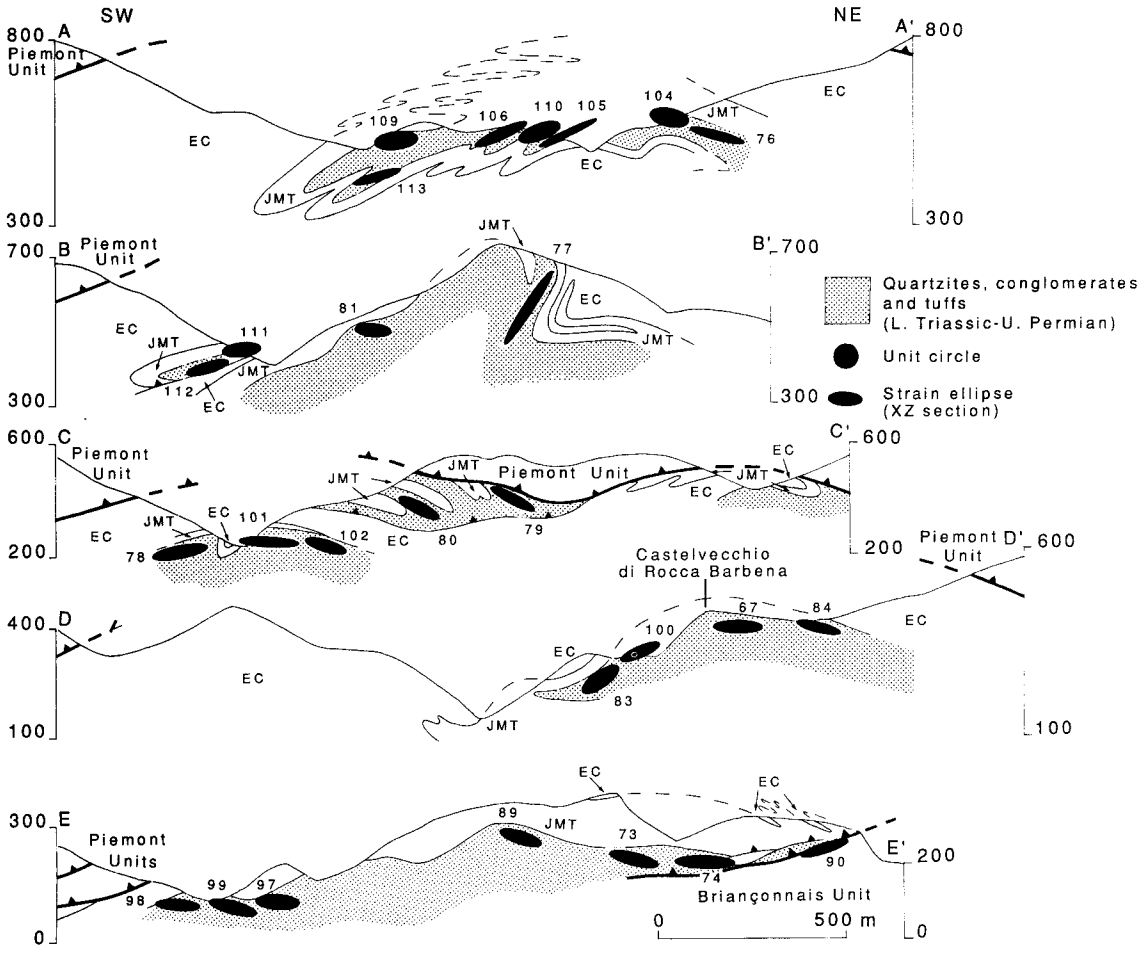

Fig. 8. Cross-sections through the CVC, more or less parallel to the stretching lineation, hence to the inferred direction of nappe transport. EC: Eocene–Upper Cretaceous calc-schists. JMT: Jurassic marbles and Middle Triassic carbonates. Position of sections indicated in Fig. 6; numbers refer to the sampling sites.

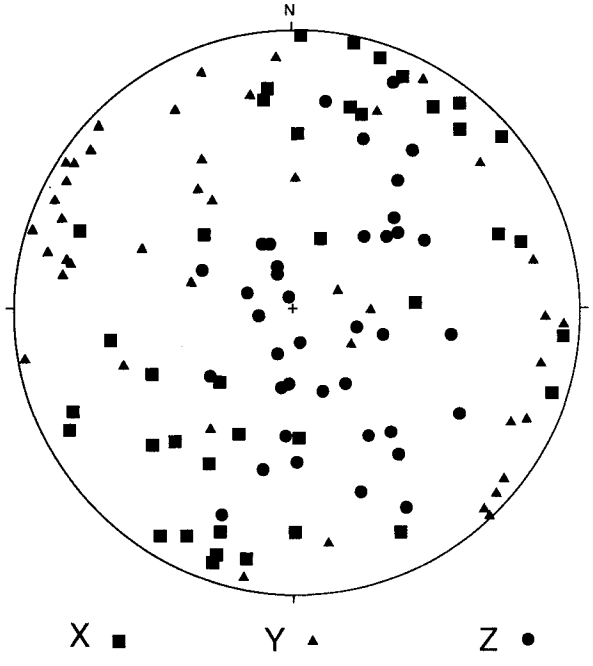

Fig. 9. Orientation of the X, Y and Z axes of the finite strain ellipsoids in the CVC. Lower-hemisphere, equal-area projection. Data from Table 2.

may fit well with a bedding-normal flattening component.

The deformation history which best accounts for the strain distribution in the CVC seems to involve (1) volume reduction, minimal in quartzites and conglomerates, and maximal in tuffs, followed by (2) a combination of simple shear and extension parallel to the layer.

Tectonic implications

The calc-schists, representing the statigraphic top of the CVC, are Upper Cretaceous–Lower Eocene in age: there are no tectonic deformations confined in the pre-Eocene part of the succession. Consequently the CVC started to deform at the Middle Eocene, when a décollement surface was formed at the base of Verrucano and Permian tuffs. As the CVC is now placed below a stack of larger nappes including Piemont and Helminthoid flysch units, it probably moved southwestward when it was incorporated into this nappe complex, previously piled up and travelling on the Briançonnais units from NE to SW. Within the nappe this deformation was generally accommodated by a subhorizontal ductile shear, parallel to the layers: field evidence and finite

strain data show that the nappe underwent extensional flow and became elongated parallel to its displacement direction. The longitudinal strain component may have reflected gravitational spreading during the final stage of nappe motion (Elliott 1976, Ramberg 1977), which was a consequence of the stacking of the Piemont and Helminthoid flysch nappes over the CVC: alternatively it could be generated during the evolution of thrust systems, i.e. antiformal stack.

On the basis of the distance of the more southwestern outcrops of the CVC and the position of its possible pre-Permian stratigraphic substratum: the minimum amount of translation parallel to the direction of movement is about 13 km. This suggests that most of the displacement was confined to the thrust fault or to ductile shear in a narrow shear zone close to the fault.

CONCLUSIONS

The interpretation of strain patterns in the CVC has led to a model in which longitudinal strain was superposed on layer-parallel simple shear. Finite strains in the Permo-Triassic sequence have been shown to result from a single deformation event corresponding to overthrusting of the CVC towards more external domains. Extension lineations, orientation of the X axes and the shear-sense indicators prove that the translation took place from NE to SW, in agreement with the tectonic history of the CVC as reconstructed from regional geological evidence (Vanossi 1980). Data presented here emphasize that subvertical thinning associated with thrust shear and a small extension perpendicular to the emplacement direction occurred. Although locally folded, the CVC maintains a thrust sheet geometry showing the lack of an extensive inverted limb: this results in the observed homogeneity of strain intensity across the nappe.

Many nappes dominated by overthrust tectonics present a complex distribution of the strain (Hossack 1968, Coward & Kim 1981, Kligfield *et al.* 1981, Platt & Behrmann 1986), approximately similar to that in the CVC. In some cases it has been shown that the coexistence of oblate and prolate ellipsoids has mainly a structural control: local constriction or flattening fields can, for example, be produced by superposed deformations related to shear zone and thrust terminations (Ramsay & Allison 1979, Coward & Potts 1983), or with differential movement inside the shear zones (Hudleston 1983). I would like to emphasize that the finite

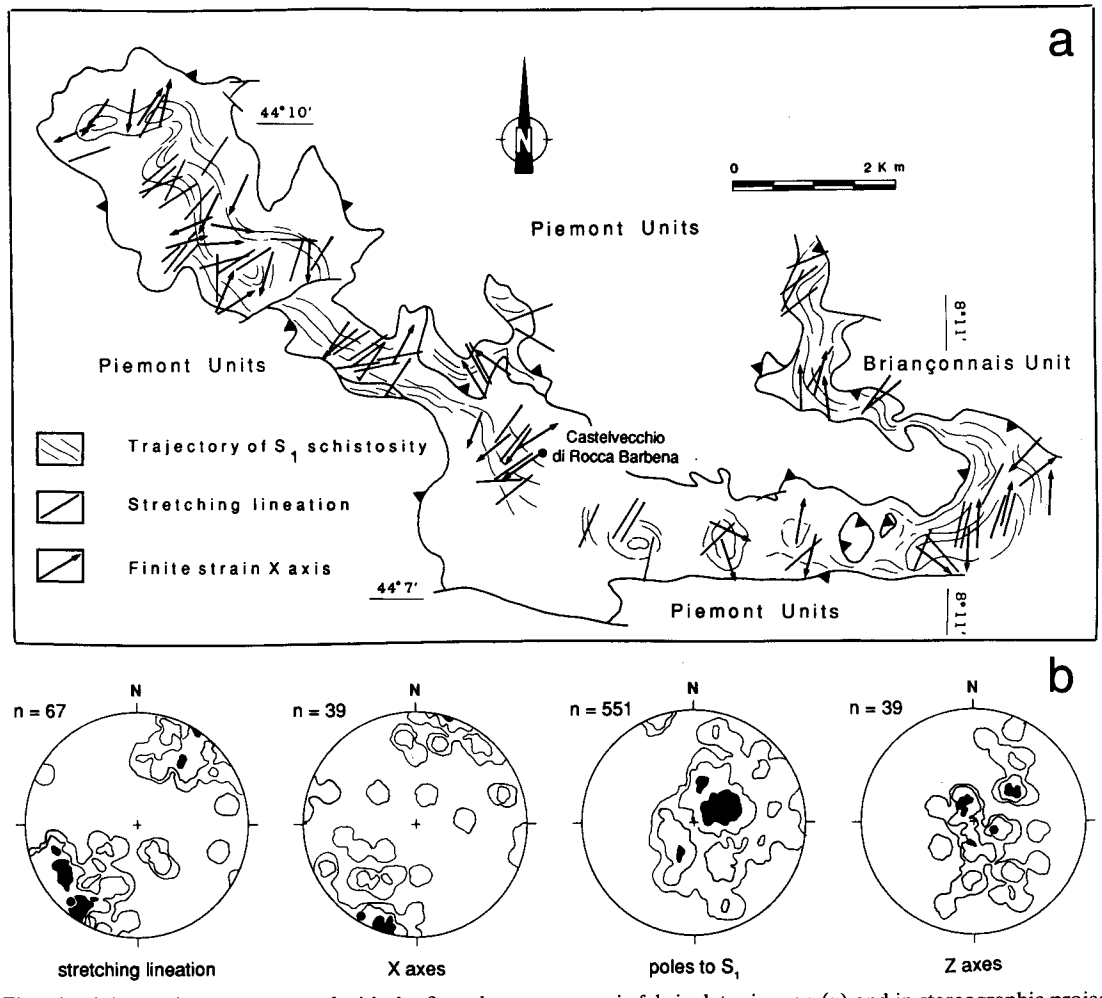

Fig. 10. Finite strain axes compared with the first-phase mesoscopic fabric data, in map (a) and in stereographic projections (b). Contours 2, 6 and 14% of data points per 1% area; black circle indicates the mean vector of linear elements (lower-hemisphere equal-area projections).

Table 3. Possible strain factorization in pre-tectonic compaction and tectonic plane strain. Compaction is given in terms of per cent shortening along Z. See text for discussion

Sample	Rock type	K	% Compaction	Plane strain (X/Z)
SCV 70	Tuff	0.49	−0.35	5.51
SCV 76	Conglomerate	0.95	−0.03	5.60
SCV 79	Tuff	0.68	−0.25	4.68
SCV 80	Conglomerate	0.93	−0.06	3.63
SCV 81	Conglomerate	0.28	−0.45	2.91
SCV 84	Tuff	0.64	−0.27	4.09
SCV 85	Tuff	0.57	−0.33	4.30
SCV 89	Quartzite	0.79	−0.13	3.40
SCV 90	Conglomerate	0.58	−0.34	4.74
SCV 91	Tuff	0.96	−0.03	4.12
SCV 94	Tuff	0.31	−0.62	6.32
SCV 96	Tuff	0.82	−0.23	14.68
SCV 98	Tuff	0.52	−0.34	3.77
SCV 100	Tuff	0.48	−0.37	3.55
SCV 101	Tuff	0.84	−0.15	6.18
SCV 102	Tuff	0.33	−0.50	3.93
SCV 105	Tuff	0.45	−0.56	9.10
SCV 111	Conglomerate	0.96	−0.02	2.69
SCV 112	Conglomerate	0.43	−0.43	3.91
SCV 113	Tuff	0.34	−0.57	5.51

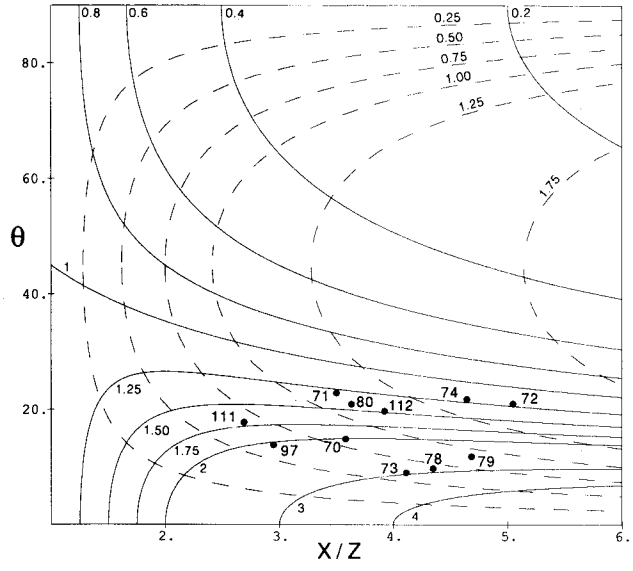

Fig. 11. X/Z ratios plotted against the angle θ between the X axes and the major thrust boundaries of the CVC (Coward & Kim 1981, Kligfield *et al.* 1981, Sanderson 1982). All the data show an extra extension in the X direction.

strains examined in this study reflect first of all a lithologically controlled partitioning of deformation: this fact poses serious constraints and suggests great caution is needed in the correlation between strain data and the major structural features of the CVC.

Acknowledgements—I wish to thank M. Vanossi for discussions and helpful criticism of the manuscript; D. Sanderson and two anonymous referees for their careful review; U. Croce for technical assistance. This research was supported by the C.N.R. (project 'Problemi geologici della regione alpino-padana') and by a M.U.R.S.T. 40% grant (arranged by G. Cassinis).

REFERENCES

Athy, L. F. 1930. Density, porosity, and compaction of sedimentary rocks. *Bull. Am. Ass. Petrol. Geol.* **14**, 1–24.

Baldwin, B. & Butler, C. O. 1985. Compaction curves. *Bull. Am. Ass. Petrol. Geol.* **69**, 622–626.

Berthé, D., Chouckroune, P. & Jegouzo, P. 1979. Orthogneiss, mylonite and non-coaxial deformation of granites: the example of the South Armorican Shear-Zone. *J. Struct. Geol.* **1**, 31–42.

Consiglio Nazionale delle Ricerche 1983. Neotectonic map of Italy. *Quaderni La Ricerca Scientifica* **114**.

Coward, M. P. & Kim, J. H. 1981. Strain within thrust sheets. In: *Thrust and Nappe Tectonics* (edited by McClay, K. R. & Price, N. J.). *Spec. Publs geol. Soc. Lond.* **9**, 275–292.

Coward, M. P. & Potts, G. J. 1983. Complex strain patterns developed at the frontal and lateral tips to shear zones and thrust zones. *J. Struct. Geol.* **5**, 383–399.

Crespi, J. M. 1986. Some guidelines for the practical application of Fry's method of strain analysis. *J. Struct. Geol.* **8**, 799–808.

Elliott, D. 1976. The energy balance and deformation mechanisms of thrust sheets. *Phil. Trans. R. Soc.* **A283**, 289–312.

Erslev, E. A. 1988. Normalized center-to-center strain analysis of packed aggregates. *J. Struct. Geol.* **10**, 201–209.

Fry, N. 1979. Random point distributions and strain measurements in rocks. *Tectonophysics* **60**, 89–105.

Hanna, S. S. & Fry, N. 1979. A comparison of methods of strain determination in rocks from southwest Dyfed (Pembrokeshire) and adjacent areas. *J. Struct. Geol.* **1**, 155–162.

Hossack, J. R. 1968. Pebble deformation and thrusting in the Bygdin area (Southern Norway). *Tectonophysics* **5**, 315–339.

Hudleston, P. J. 1983. Strain patterns in an ice cap and implications for strain variations in shear zones. *J. Struct. Geol.* **5**, 455–463.

Kligfield, R., Carmignani, L. & Owens, W. H. 1981. Strain analysis of a Northern Apennine shear zone using deformed marble breccias. *J. Struct. Geol.* **3**, 421–436.

Lacassin, R. & van den Driessche, J. 1983. Finite strain determination of gneiss: application of Fry method to porphyroid in the southern Massif Central (France). *J. Struct. Geol.* **5**, 245–253.

Lisle, R. J. 1977. Clastic grain shape and orientation in relation to cleavage from the Aberystwyth Grits, Wales. *Tectonophysics* **39**, 381–395.

Lister, G. S. & Snoke, A. W. 1984. S–C mylonites. *J. Struct. Geol.* **6**, 617–638.

Menardi Noguera, A. 1988. Structural evolution of a Briançonnais cover nappe, the Caprauna-Armetta Unit (Ligurian Alps, Italy). *J. Struct. Geol.* **10**, 625–637.

Messiga, B., Oxilia, M., Piccardo, G. B. & Vanossi, M. 1982. Fasi metamorfiche e deformative alpine nel Brianzonese–Piemontese esterno delle Alpi liguri: un possibile modello evolutivo. *Rend. Soc. It. Miner. Petrol.* **38**, 261–280.

Passchier, C. W. & Simpson, C. 1986. Porphyroclast systems as kinematic indicators. *J. Struct. Geol.* **8**, 831–843.

Peach, C. J. & Lisle, R. J. 1979. A Fortran IV program for the analysis of tectonic strain using deformed elliptical markers. *Comput. & Geosci.* **5**, 325–334.

Perrier, R. & Quiblier, J. 1974. Thickness changes in sedimentary

layers during compaction history; methods for quantitative evaluation. *Bull. Am. Ass. Petrol. Geol.* **58**, 507–520.

Platt, J. P. & Behrmann, J. H. 1986. Structures and fabrics in a crustal-scale shear zone, Betic Cordillera, SE Spain, *J. Struct. Geol.* **8**, 15–33.

Ramberg, H. 1977. Some remarks on the mechanism of nappe movement. *Geol. För. Stockh. Förh.*, 110–117.

Ramsay, J. G. 1967. *Folding and Fracturing of Rocks*. McGraw-Hill, New York, 1–568.

Ramsay, J. G. 1980. Shear zone geometry: a review. *J. Struct. Geol.* **2**, 83–89.

Ramsay, J. G. & Allison, I. 1979. Structural analysis of shear zones in an Alpinized Hercynian granite, Maggia Lappen, Pennine Zone, Central Alps. *Schweiz. miner. petrogr. Mitt.* **59**, 251–279.

Ramsay, J. G. & Huber, M. I. 1983. *The Techniques of Modern Structural Geology, Volume* 1: *Strain Analysis*. Academic Press, London.

Roberts, B. & Siddans, A. W. B. 1971. Fabric studies in the Llwyd Mawr ignimbrite, Caernarvonshire, North Wales. *Tectonophysics* **12**, 283–306.

Sanderson, D. J. 1976. The superposition of compaction and plane strain. *Tectonophysics* **30**, 35–54.

Sanderson, D. J. 1982. Models of strain variation in nappes and thrust sheets: a review. *Tectonophysics* **88**, 201–233.

Schwerdtner, W. M., Stott, G. M. & Suttcliffe, R. H. 1983. Strain patterns in crescentic granitoid plutons in the Archean greenstone terrain of Ontario. *J. Struct. Geol.* **5**, 419–430.

Seno, S. 1988. Strutture interne e meccanismi di deformazione in una falda Brianzonese: l'esempio dell'unità di Castelvecchio–Cerisola. *Boll. Soc. Geol. It.* **107**, 453–470.

Seno, S. & Turrini, C. 1989. Sistemi di vene di estensione e scistosità in formazioni calcareo-argillose. *Boll. Soc. Geol. It.* **108**, 687–697.

Shimamoto, T. & Ikeda, Y. 1976. A simple algebraic method for strain estimation from deformed ellipsoidal objects. 1. Basic theory. *Tectonophysics* **36**, 315–337.

Siddans, A. W. B., Henry, B., Kligfield, R., Lowrie, W., Hirt, A. & Percevault, M. N. 1984. Finite strain patterns and their significance in Permian rocks of the Alpes Maritimes (France). *J. Struct. Geol.* **6**, 339–368.

Simpson, C. & Schmid, S. M. 1983. An evaluation of criteria to deduce the sense of movement in sheared rocks. *Bull. geol. Soc. Am.* **94**, 1281–1288.

Stone, D. & Schwerdtner, W. M. 1981. Total strain within a major mylonite zone, southern Canadian Shield. *J. Struct. Geol.* **3**, 193–194.

Thiessen, R. L. & Means, W. D. 1980. Classification of fold interference patterns: a reexamination. *J. Struct. Geol.* **2**, 311–316.

Tullis, J., Christie, J. M. & Griggs, D. T. 1973. Microstructures and preferred orientations of experimentally deformed quartzites. *Bull. geol. Soc. Am.* **84**, 297–314.

Vanossi, M. 1980. Les unités géologiques des Alpes Maritimes entre l'Ellero et la mer Liqure: un aperçu schématique. *Mem. Soc. Geol. Padova* **34**, 101–142.

Vanossi, M., Cortesogno, L., Galbiati, B., Messiga, B., Piccardo, G. & Vannucci, R. 1986. Geologia delle Alpi Liguri: dati, problemi, ipotesi. *Mem. Soc. Geol. It.* **28**, 5–75.